You, Z.; Behl, M.; Grage, S.; Bürck, J.; Zhao, Q.; Ulrich, A.; Lendlein, A.:
Shape-Memory Effect by Sequential Coupling of Functions over Different Length Scales in an Architectured Hydrogel.
In: Biomacromolecules. Vol. 21 (2020) 2, 680 - 687.

First published online by ACS: 17.12.2019

https://dx.doi.org/10.1021/acs.biomac.9b01390

Shape-memory Effect by Sequential Coupling of Functions over Different Length Scales in an Architectured Hydrogel

*Zewang You[1,2,3], Marc Behl[1,3], Stephan L. Grage[4], Jochen Bürck[4], Qian Zhao[6], Anne S. Ulrich[4,5], and Andreas Lendlein[1,2,3] **

[1] Institute of Biomaterial Science, Helmholtz-Zentrum Geesthacht, Kantstraße. 55, 14513 Teltow, Germany
[2] Institute of Chemistry, University of Potsdam, Karl-Liebknecht-Straße. 24-25, 14476 Potsdam, Germany
[3] Tianjin University – Helmholtz-Zentrum Geesthacht Joint Laboratory for Biomaterials and Regenerative Medicine, Weijin Road 92, 300072 Tianjin, China and Kantstraße. 55, 14513 Teltow, Germany
[4] Institute of Biological Interfaces (IBG-2), Karlsruhe Institute of Technology (KIT), POB 3640, 76021 Karlsruhe, Germany
[5] Institute of Organic Chemistry, Karlsruhe Institute of Technology (KIT), Fritz-Haber-Weg 6, 76131 Karlsruhe, Germany
[6] State Key Laboratory of Chemical Engineering, College of Chemical and Biological Engineering, Zhejiang University, Hangzhou, 310027 PR China

ABSTRACT: The integration of functions in materials in order to gain macroscopic effects in response to environmental changes is an ongoing challenge in material science. Here, functions on different hierarchical levels are sequentially linked to translate a pH-triggered conformational transition from the molecular to the macroscopic level to induce directed movements in hydrogels. When the pH is increased, lysine-rich peptide molecules change their conformation into a β-hairpin

structure due to the reduced electrostatic repulsion amongst the deprotonated amino groups. Coupled to this conformation change is the capability of the β-hairpin motifs to subsequently assemble into aggregates acting as reversible crosslinks, which are used as controlling units to fix a temporary macroscopic shape. A structural function implemented into the hydrogel by a microporous architecture enabled non-disruptive deformation upon compression by buckling of pore walls as well as their elastic recovery. Coupled to this structural function is the capability of the porous material to enhance the diffusion of ions into the hydrogel and to keep the dimension of the macroscopic systems almost constant when the additional crosslinks are formed or cleaved as it limits the dimensional change of the pore walls. Covalent crosslinking of the hydrogel into a polymer network acted as gear shift to ensure translation of the function on the molecular level to the macroscopic dimension. In this way the information of a directed shape-shift can be programmed into the material by mechanical deformation and pH-dependent formation of temporary netpoints. The information could be read out by lowering pH. The peptides reverted back into their original random coil conformation and the porous polymer network could recover from the previously applied elastic deformation. The level of multifunctionality of the hydrogels can be increased by implementation of additional orthogonal functions like antimicrobicity by proper selection of multifunctional peptides, which could enable sophisticated biomedical devices.

Keywords: shape-memory effect, cryogel, stimuli-sensitive peptide, pH-triggered, shape programmable material, architectured hydrogel

INTRODUCTION

The amplification of processes occurring on the molecular level, such as changes of the conformation to induce macroscopic changes by translation through coupling over several levels of hierarchy, is the supreme discipline to gain multifunctional smart materials.[1] Validity of this concept has been demonstrated on liquid-crystalline elastomers with incorporated azobenzene moieties, in enantiomeric forms of adsorbed organic molecules or by DNA carbon nanotube hybrids.[2-6]

However, in these systems so far, only the sequentially coupling of the molecular switching function in terms of an amplification of a molecular effect could be demonstrated, in some cases even over several levels of hierarchy. But the realization of different effects (such as shape programmability or shape-memory effects) by coupling the molecular switching function with other functions like the structural function of an architectured hydrogel or switchable chain mobilities could not yet be realized. In aqueous environments, the swelling impedes orientation of the coupled switches and consequently directed movement. Reprogrammable directed shape-shifts demand sequentially linked molecular switching functions to be translated over several levels of hierarchy and to be coupled in, and to be processed by the macroscopic directed shape-shift function. Reprogrammable directed shape-shifts in swollen polymeric systems could be realized in shape-memory hydrogels (SMHs), which can

be programmed into a temporary shape that can be reversed when a suitable stimulus like heat is applied.[7-10] Promising pH-sensitive switches for aqueous environments are biomolecules like peptides, enzymes or DNA sequences, which respond to changes of pH by a change of conformation.[11-15]

We have asked ourselves whether a multifunctional swollen material could be designed in which the reversible conformational change of the biomolecule would be sequentially coupled by a sophisticated design over several levels of hierarchy to trigger a macroscopic reprogrammable directed shape-shift.

Among the switchable biomolecules, peptides are interesting building blocks for the molecular switching function as they respond to changes of the environment by transitioning into unique conformational motifs such as β-sheet, α-helix or coil structures.[16, 17] The conformational change is caused by the attraction or repulsion of positively or negatively charged amino acid residues and therefore depends on the amino acid itself, as well as on the sequence of amino acids.

Accordingly, a first sequential translation conformational change of the peptides into β-hairpin conformation should be realized by their subsequent self-assembly acting as reversible additional crosslinks, which increases the modulus. This increase in modulus should couple into the reprogrammable shape-shifting function, demanding an amplification of the signal from the morphological to the macroscopic level. It was speculated that this coupling over hierarchy and coupling to the shape-shifting function could be reached by a skeleton provided by a microporous structure created by UV-

initiated cryo-polymerization.[18-20] Here, the microporous architecture should enable compressibility of the material by buckling of the pore walls once the information of the defined shape-shift and reprogrammability by the elastic recovery of the deformed pore walls. Furthermore, the porous structure was supposed to address the need of fast diffusion of ions into the hydrogel. Linked to this function was the volume stability as the pores also prevented the water being squeezed out of the swollen polymer network and limited the changes in swelling once the peptide aggregates are cleaved to the pore walls.

Covalent crosslinking of the hydrogel into a polymer network, which is capable to reverse a deformation by elastic recovery and in this way enables a directed movement, was supposed to act as gear shift to ensure translation of the molecular switching function to the macroscopic dimension. The covalent attachment of the peptides should ensure the reversibility of the system, as compared to other stimuli-sensitive gels, no complexing agents or ions can be leached out.

When the peptide segments have a random conformation, the hydrogel is elastic and can be deformed into a temporary shape. Increase of the pH causes a conformational change of the peptides into a β-hairpin structure and their subsequent assembly acts as additional crosslinks, which hinder elastic recovery of the polymer network. A potential candidate material for the switching peptide is the peptide MAX1 (VKVKVKVKVpPTKVKVKVKV-NH_2), which adopts random coil conformation at pHs below 5.5 and changes its conformation into a β-hairpin structure when the pH is

raised to 9. The driving force for the conformational change is the elimination of electrostatic repulsion between protonated lysines upon increased pH. This conformational change is accompanied by a self-assembly resulting in a physical hydrogel network under basic conditions due to the facial hydrophobic interactions and hydrogen bonds, which dissolve under acidic conditions by adopting a random coil conformation. In case of the deformed peptide hydrogels, the change into random conformation of the peptides upon decreasing the pH results in elastic recovery of the polymer network as the additional crosslinks fixing the deformation are cleaved. The elastic recovery is supported by the geometry mechanics of the micropores to recover their original shape. In addition, this porous microstructure limits the change of the macroscopic hydrogel volume throughout the shape-memory effect to the pore walls.[21]

As a matrix material for the pore walls of the cryogels, we selected a copolymer network composed of a hydrophilic cross-linkable oligomer precursor and a pH-sensitive peptide acting as switching segments. The pH-sensitive peptides were incorporated as grafted side chains to minimize the influence on swelling when switching occurs. Poly(ethylene glycol) dicarbamatoethyl methacrylate (PEGdiCEMA, M_n = 4,000 g·mol^{-1}) was selected as hydrophilic, crosslinkable precursor and was copolymerized with the peptide sequence VK20[22], which is based on the peptide MAX1 but provides a methacrylate terminal group (CH_2=C(-CH_3)-CO-NH-VKVKVKVKVpPTKVKVKVKV-NH_2) (Figures 1 and S1). This derivative of MAX1 was selected, as it is highly soluble in water and capable of folding reversibly - at first

into a *β*-hairpin structure and then self-assemble upon altering the pH. Under acidic conditions, the lysine side chains in MAX1 are protonated (with a net charge of +9), which prevents the peptide from folding and thus self-assembling. Once the pH is increased to 9, the peptide adopts a *β*-hairpin structure.

Structure-function relationships of this pH-sensitive architectured hydrogel system (cryogel) were explored by the synthesis of several series of peptide cryogels VKx(y), in which the weight content of peptide (*x*) and the weight content of crosslinker relative to the peptide content (y) were varied (Table S1). The obtained hydrogels were characterized with regard to the conformational transition of peptides at the molecular level, the porous structure at the micro level, and the swelling behavior and mechanical properties at the macro level. The capability of pH-triggered SME of these cryogels was investigated and the shape-memory capability was quantified. Furthermore, the nanostructure of the peptide switching domains was studied by neutron scattering techniques to further elucidate the molecular mechanism of SME, in which the reversible conformational transition of peptides acts as a switch.

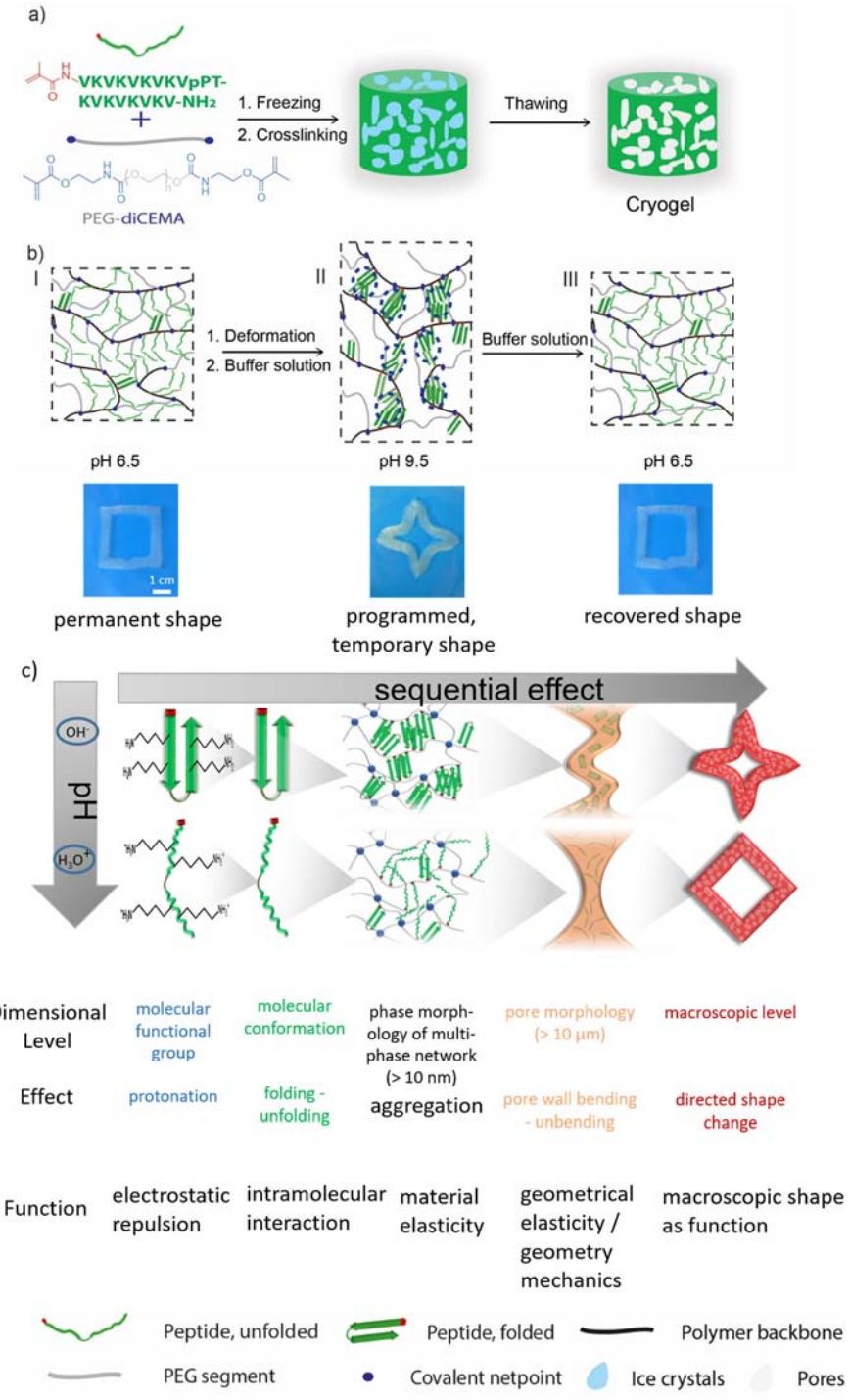

Figure 1. pH-triggered SME of peptide-based cryogel. a) Microporous peptide containing cryogels were created by UV-initiated cryo-polymerization; b) schematic and macroscopic representation of the shape-memory effect. Images of VK3(67) peptide cryogel showing the SME (second cycle) I) permanent shape at pH 6.5; II) temporary shape at pH 9.5; III) recovered shape at pH 6.5. c) Sequential coupling of functions: conformational change of the peptide segments is capable of fixing a deformation. When the pH is increased, the switching function by the conformational change of the peptides into β-hairpin structure occurs, which is sequentially translated

to the morphological level by their subsequent assembly, which acts as additional crosslinks. When the pH is lowered again the peptides re-adopt a random conformation, resulting in elastic recovery of the polymer network and by this unbuckling of the pores. In this way, the conformational change of the peptide is translated to the macroscopic systems, causing shape recovery of the foam.

EXPERIMENTAL METHODS

Materials:

2-N-morpholino ethanesulfonic acid (MES), boric acid, D_2O, NaOD (40 wt% D_2O solution), DCl (35 wt% D_2O solution), and Congo red were purchased from Sigma-Aldrich (Taufkirchen, Germany). Buffer solutions were prepared by dissolving MES or boric acid with Milli-Q water, pH was adjusted by titration with NaOH. The following buffer solutions were used for the pH ranging between 6 and 10: pH 6 (MES), pH 6.5 (MES), pH 8.5 (boric acid), pH 9 (boric acid), pH 9.5 (boric acid), and pH 10 (boric acid). Methacrylated peptide sequences (VK20, NK8) were purchased from Smartox Biotechnology (Saint Martin d'Hères, France) and Phtd Peptides Co., Ltd (Zhengzhou, China). 2-isocyanatoethyl methacrylate (IEMA), dibutyltin dilaurate were purchased from Sigma-Aldrich (Steinheim, Germany) and used as received. Polyethylene glycol (PEG, M_n = 4000 g·mol^{-1}) was purchased from Merck (Darmstadt, Germany). Poly (ethylene glycol) dicarbamatoethyl methacrylate (PEGdiCEMA, M_n = 4000 g·mol^{-1}) was synthesized according to the procedure reported in the supporting reference.[10] Irgacure 2959 (1-[4-(2-Hydroxyethoxy)-phenyl]-2-hydroxy-2-methyl-1-propane-1-one) was a gift from BASF (Ludwigshafen, Germany).

Synthesis:

Porous hydrogels were synthesized by frozen-UV cryo-polymerization. A general procedure is as follows. At first the peptide monomer and the corresponding amount of crosslinker were dissolved in Milli-Q water. A photoinitiator solution containing 3 wt% Irgacure 2959 was prepared in a mixture of ethanol/water (V/V = 1:1) and added in a concentration of 1 wt% to the peptide monomer. The peptide monomer/photoinitiator mixture was carefully injected with a syringe into molds from aluminum foil. The molds were cooled by positioning above liquid nitrogen until the mixture was frozen and then placed under an Excimer Laser (Bluelight PS 30P Excimer laser, λ = 308 nm, 50 W, Heraeus Noblelight, Germany) at a distance of 7.5 cm, with a current of 4.5 A. The content of the molds was irradiated for 60 min. Afterwards, the samples were extracted with water, which was exchanged every 12 h at least 6 times to remove unreacted moieties until equilibrium swelling was reached.

Methods:

IR spectra were collected on a Nicolet IR 6700 spectrometer equipped with an Attenuated Total Reflection (ATR) unit. Peptide NK8 solution was prepared by dissolving the deuteriochloride salt of solid NK8 in D_2O, resulting in a 1 wt% solution. A small amount of concentrated NaOD was added to increase the pH to 10. Deuterated VK20 * nDCl was prepared by lyophilizing the TFA salt of the peptide from 0.1 M DCl. For peptide cryogels, the samples were immersed 12 h in the buffer solutions before measurement to ensure the equilibrium of conformational change. To estimate

the conformation of peptide segments, the obtained spectra were analyzed using PeakFit 4.12 software (SeaSolve Software Inc., Framingham, United States of America). The amide I region (1580-1740 cm^{-1}) was deconvolved by Gauss Amplitude function after a linear baseline correction. For the curve-fitting procedure, the automated second derivative method was applied, in which the band widths were kept constant. The optimal fit divided the original spectra into individual Gaussian peaks. In this way, the absorption peaks of random coil (1645 cm^{-1}) and *β*-sheet (1620 cm^{-1}) conformation were separated and the peak areas ($A_{\beta\text{-sheet}}$ and $A_{\text{random coil}}$) can be used to calculate the relative *β*-sheet content X_β by using the following equation:

$$X_\beta = A_{\beta\text{-sheet}} / (A_{\beta\text{-sheet}} + A_{\text{random coil}}) * 100\%.$$

Binding study: small pieces of the peptide cryogels were exposed to 10 ml of a 0.1 wt% solution of Congo red in water.

Ultraviolet visible (UV-VIS) absorption spectra were recorded with a Cary 100 spectrophotometer (Agilent, Darmstadt, Germany) at ambient temperature (20 °C). The gel samples were placed in a solid sample holder with an aperture of 1 mm. The absorption spectra were recorded in the range of 300-700 nm.

Circular dichroism (CD) spectra were collected on a J-1500 spectropolarimeter (Jasco, Hachioji, Japan). Peptide NK8 solution was prepared by dissolving the 0.05 wt% NK8 in milli-Q water. The NK8 solution was transferred to a 1 mm quartz cell. A small amount 0.1 M NaOH was added to increase the pH. The temperature was kept constant at 25 °C.

Synchrotron radiation circular dichroism (SRCD) spectra were recorded at the UV-CD 12 beamline with experimental setups installed at the KARA Synchrotron Radiation Facility (Karlsruhe, Germany). Prior to the cutting procedure the peptide cryogels were immersed in buffer solutions of pH 6.5 and 9.5. The swollen peptide cryogels were cut into slices of 30 μm thickness by using a CM 1900 cryo-microtrome (Leica, Nussloch, Germany). The cryogel slices were transferred into the demountable CaF_2 cells with path lengths of 12.0 $\pm$ 0.2 μm or 14.6 $\pm$ 0.2 μm. Cells were mounted in a sample holder and then fitted in the SRCD module consisting of a U-shaped copper block. The holder was temperature-controlled by two Peltier heat pumps. Spectra were recorded at four angles (0°, 90°, 180°, and 270°) sequentially, while the sample holder was rotated at 15 °C to eliminate the artifacts of linear dichroism. All spectra are the average data of four measurements. The mean residue ellipticity [θ] was calculated from the equation $[\theta]=(\theta_{obs}/10lc)/n$, where θ_{obs} is the measured ellipticity in millidegrees, l is the path length of the cell in centimeters, c is the concentration in molar, and n is the number of residues.

Solid-state NMR measurements were carried out on a Bruker Avance 500 MHz spectrometer (Bruker Biospin, Karlsruhe, Germany) equipped with a 4 mm Bruker magic angle spinning (MAS) probe at 25 °C. Single-pulse excitation experiments were performed for peptide cryogels VK4(50) and PEG cryogels at pH 6.5 and 9.5. The ^{13}C chemical shifts reported for peptide cryogels are relative values, relative to the internal

PEG signal. The single-pulse excitation spectra were acquired at a MAS frequency of 8 kHz for all samples.

WAXS measurements were conducted at ambient temperature in transmission geometry utilizing X-ray diffraction system Bruker D8 Discover (generator operated at 40 kV and 40 mA) with a two-dimensional detector (Bruker AXS, Karlsruhe, Germany). The X-ray beam (Cu $K\alpha_1$ radiation, λ = 0.154 nm) was provided by a graphite monochromator and a pinhole collimator with an opening of 0.8 mm. Sample-to-detector distance was 15 cm applying an irradiation time of 120 seconds. Integration of the 2-D intensities gave linear intensity curves I (2θ).

The *SANS measurements* were conducted on the small-angle neutron scattering instrument SANS-1 at FRM II (Forschungsneutronenquelle Heinz Maier-Leibnitz, Garching, Germany). The peptide VK20 was dissolved in D_2O and then mixed with pH 6.5 and pH 9.5 buffer solutions, resulting in 1 wt% VK20 solution at pH 6.5 and 1 wt% VK20 gel at pH 9.5. The samples were transferred into quartz cuvettes with 1 mm path length for the measurements. The 1 wt% VK20 gel was incubated at pH 9.5 for 2 h to allow the complete gelation before the measurements. In the case of cryogels, peptide cryogel VK4(50) and PEG cryogels were immersed in pH 6.5 and 9.5 solutions overnight. The samples were transferred into a sample holder consisting of two pieces of aluminum foils (1 cm diameter) with a 1 mm O-ring spacer in between. Spectra were obtained at room temperature and were collected for 150 minutes per sample. The sample to detector distances were 2 m, 8 m, and 20 m, resulting in Q range for these

measurements of 0.001 Å to 0.4 Å. Data-reduction and normalization were performed using standard techniques via BerSANS software [23] (Hahn-Meitner-Institute, Berlin, Germany). Standard Guinier analysis[24] was used to calculate the radius of gyration of peptide VK20 at pH 6.5 solution via the equation of $\ln[I(Q)] = \ln[I_0] - Q^2R_g^2/3$. For the physical VK20 gel at pH 9.5, a modified Guinier analysis[22] for rod-like objects was adapted, the form factor $P(Q) \propto (1/Q) \exp[(-Q^2R_g^2)/2]$, where R_g is the cross-sectional radius of gyration. The slope of the scattering data plotted as $\ln[Q*I(Q)]$ vs Q^2 gives $R_g^2/2$, and the radius of rod cross section, $r = R_g\sqrt{2}$.

SEM measurements were performed with a desktop-SEM Phenom G2 from PhenomWorld (LOT-Oriel Group Europe, Darmstadt, Germany). Briefly, the samples were firstly lyophilized in a freeze-dryer. When constant weight was achieved, the samples were sputtered with 5 nm gold prior to SEM imaging. Light microscopy (Axio Imager, Carl Zeiss Microimaging, Göttingen, Germany) was used to investigate the porous structure of 50 μm cryo-slices of cryogels swollen to equilibrium in water at 25 °C.

Rheological investigations were performed on a Haake Rheowin Mars III (Thermo Scientific, Karlsruhe, Germany) by using a 20 mm plate-plate geometry at 25 °C. The cryogels were firstly analyzed by amplitude sweeps over a strain range of 0.01% to 10% to determine the linear viscoelastic regions. Frequency sweep measurements of peptide cryogels were performed under constant stresses of 1 Pa within the frequency range from 0.05 to 5 Hz and a control force of 0.2 N.

Shape-memory experiments: the shape-memory properties of the cryogels were determined in bending tests: a straight strip of the cryogel was first immersed in a solution of pH 6.5 for 2 h and bent to an angle of 0°. The deformed shape was fixed by increasing the pH to basic pH conditions (pH 8.5, pH 9.0, pH 9.5, and pH 10.0) and keeping this condition for 2 h. After the removal of external force, the temporary shape was obtained and the angle θ_f between the two ends of the strips was recorded. Afterwards the pH was adjusted to 6.5 for recovery test. Photographs were taken at different time points and the angles of the bent samples were analyzed. The shape fixity ratio (R_f) was calculated as 180°- θ_f/180°. The shape recovery ratio (R_r) was calculated as (θ_r - θ_f) / 180° - θ_f.

Unless mentioned otherwise all data calculated according to equation 1 and 2 were given as mean values ± standard deviation of at least three data points. $\overline{Y}$ is the mean value, M is the number of data points, $Y\omega$ is the value of the ω^{th} measurement, and S is the standard deviation, which describes the spread of the individual values about its mean in a data set.

$$\overline{Y} = \frac{1}{M}\sum_{\omega=1}^{M} Y\omega \qquad (1)$$

$$S = \sqrt{\frac{1}{M-1}\sum_{\omega=1}^{M}\left(Y\omega - \overline{Y}\right)^2} \qquad (2)$$

RESULTS AND DISCUSSION

Figure 1c visualizes the sequentially coupling of functions and depicts the directed shape-shifts of a demonstrator (Fig. 1b) synthesized according to the procedure provided in the experimental part.

pH values 0.5 below neutral pH as well as 0.5 higher than pH 9, the reported switching ranges of MAX1 (pH 7.0 – 9.0), were selected to ensure fast switching as well as to compensate buffer solution entrapped within the hydrogel.

The cryogel in the shape of a hollow square was immersed initially in 2-(*N*-morpholino) ethanesulfonic acid (MES) buffer solution of pH 6.5 and was then deformed into a star-like shape. This deformation was fixed by exchanging the MES solution with boric acid (BA) buffer solution of pH 9.5 and keeping these conditions for a time period of 2 h. Once the external stress was removed, the temporary shape was obtained. BA buffer was selected as the intended pH 9.5 is in the middle of the buffering range of this buffer. When the star-like shape was transferred again to MES buffer solution of pH 6.5, the recovery of the original shape occurred within 2 h.

Qualification of the molecular switching function: on the molecular level, the conformational change of the peptide segments should decrease the degree of vibrational freedom and thus should be observable in the IR absorption spectra. The FTIR spectra of peptide cryogel VK4(50) displayed amide I bands at pH 6 at 1645 and 1620 cm^{-1}, but showed a significant signal centered at pH 10 at 1620 cm^{-1}. An amide I band at 1645 cm^{-1} indicated the unordered conformation of peptides, whereas at pH 10

the band shifted to a large extent to 1620 cm^{-1}, suggesting a dominant β-sheet structure (Figure 2a and 2b).[22] The downshift of the band can be attributed to the formation of hydrogen bonding in a β-sheet structure, which affects the amide vibrations in the peptide backbone.[25] This downshift is consistent with the impact of β-sheet formation for other peptides [26] and the pH-dependent behavior of the monomer VK20.[27] The ratio of peptide segment conformations was estimated by comparing the relative area of random coil and β-sheet conformation. The percentage of the peptide segments switching reversibly between random coil and β-sheet conformation, when the pH was raised from pH 6.5 to 9.5, was 33 ± 2%. This lower degree of switching than the theoretical 100% was attributed to the confined arrangement of the peptides within the polymer network. In a kinetics study, the conformational change of VK4(50) occurred within ~120 min in the direction of β-sheet formation (pH 6.5→9.5) and required ~70 min for the cleavage (Figure S2). Furthermore, the assumption of formation of β-sheet was supported by Wide Angle X-ray Scattering (WAXS) (Figure S3) and a Congo red binding study (Figures S4 and S5).

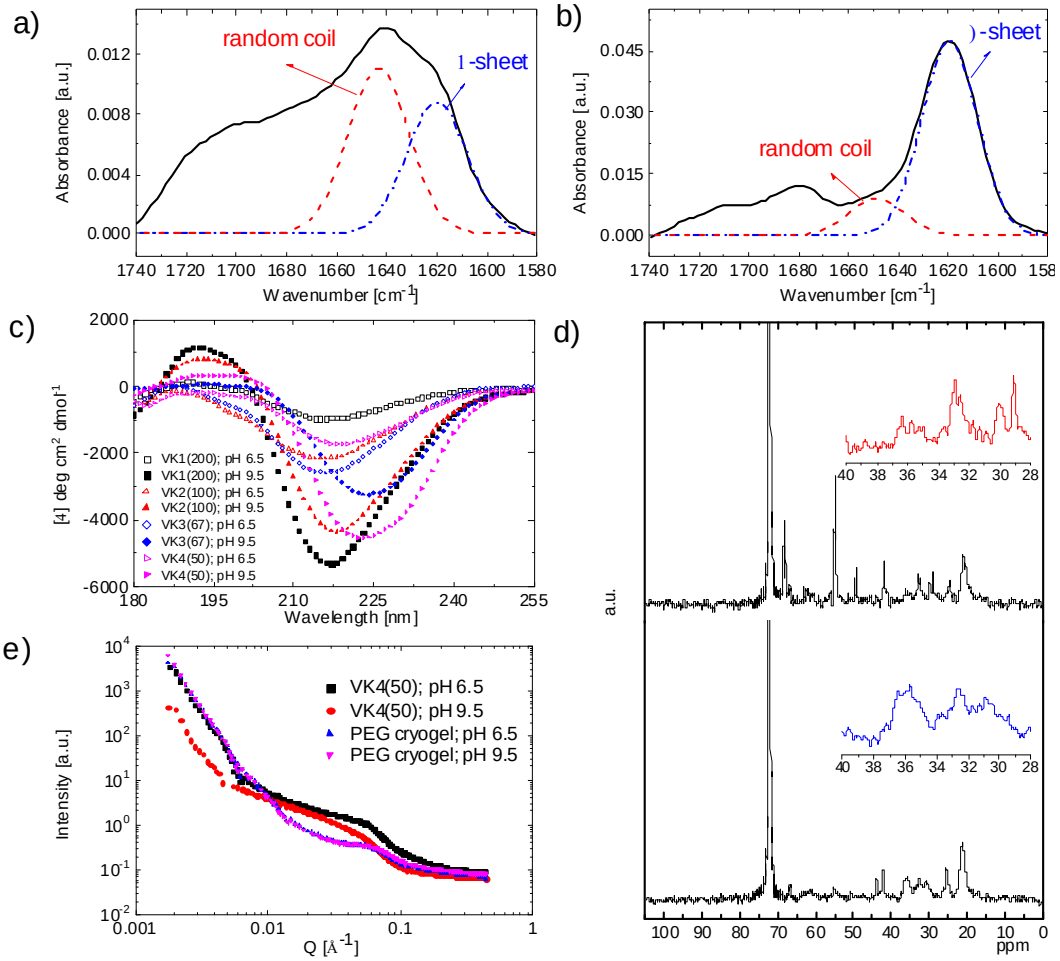

Figure 2 IR, SRCD, solid-state NMR, and SANS characterization of peptides containing cryogels at different pH values. a) IR spectra of peptide cryogel VK4(50) depicting amide I band at pH 6 (black solid line); b) at pH 10 (black solid line), the signal centered at 1646 cm^{-1} (red dashed line), and 1620 cm^{-1} (blue dash-dotted line); c) SRCD spectra of the peptide containing cryogels; d) ^{13}C single pulse excitation spectra of peptide cryogel VK4(50) (pH 6.5: upper spectrum, pH 9.5: bottom spectrum) and the magnified spectra of chemical shifts from 40 to 28 ppm; e) neutron scattering patterns of peptide cryogel VK4(50) and PEG cryogels.

The switching function based on the conformational change of peptide containing cryogels was studied in depth by synchrotron radiation circular dichroism (SRCD), which provides a higher signal to noise ratio compared to standard circular dichroism. At pH 6.5, the minimum peak at 198 nm and minimum peak centered at 216 nm indicate a mixture of random coil and β-sheet conformation of the peptide segments (Figure 2c).

At pH 9.5, the negative signals at 216 nm were significantly lower for all cryogels, which suggests predominant *β*-sheet conformation of the peptides. This result is consistent with IR studies, which confirmed the conformational transition. Furthermore, the absorption maximum at pH 9.5 correlating to *β*-sheet conformation, shifted from 216 nm to 222 nm for the cryogel compositions VK3(67) and VK4(50) with high peptide content, indicating an aggregation of *β*-sheets when the peptide concentration increased. The results qualitatively indicated the conformational transition between random coil and *β*-sheet and the subseqent assembly of individual *β*-sheets within cryogels.

Further evidence of the molecular switching function by conformational change of peptides was gained by investigating the secondary structures of peptide containing cryogels by solid-state NMR, in which single pulse excitation measurements of peptide cryogels and PEG cryogels were performed. The chemical shifts of relevant carbon atoms of the amino acid residues were assigned and listed in Table S2. The strong peaks observed in the single pulse spectra of cryogels (Figure 2d) at around 73 ppm at pH 6.5 and at 9.5 were assigned to signals from PEG. The C_β signals of valine and lysine residues displayed two peaks at 33-36 ppm. The random coil signal of C_β at the upfield was the predominant signal at pH 6.5 but significantly decreased at pH 9.5. The *β*-sheet signals shifted downfield, which agrees with the findings reported in reference[28]. *β*-sheet and random coil conformation was quantified by the integration of two peaks of C_β. The dominating random coil fraction was 63 ± 4% at pH 6.5 but decreased to

35 ± 2% at pH 9.5. This slightly higher content of random coil conformation present at both pH 6.5 and 9.5, compared to the results from FTIR measurements, can be attributed to the higher mobility of the segment in random coil conformation when compared to the *β*-sheet conformation, and is more pronounced in NMR than FTIR measurements. Nevertheless, the increase of 28 ± 3% *β*-sheet content at an increasing pH from 6 to 9.5 was consistent with the results obtained by IR measurements. In summary, the conformational transition of the peptide segments is still present within cryogel and it occurs only partially because of the restricted mobility within the hydrogel networks.

Structural investigations of peptide cryogels, and PEG cryogels in the swollen state were performed by means of Small-angle Neutron Scattering (SANS) (Figure 2e) to gain a deeper understanding of the sequentially coupling of functions. The spectra of PEG cryogels at pH 6.5 and 9.5 are almost similar, which confirms the expected insensitivity of PEG cryogels towards a pH change in this range. The spectra of VK4(50) at pH 6.5 and 9.5 exhibited quite different scattering signals in the *Q* range between 0.01 and 0.1 Å, which may hint at a conformational change of the incorporated peptide segments. In case of VK4(50) a broad shoulder was detected at pH 6.5, which can be attributed to a homogeneous distribution of the features formed as well as a fairly uniform mesh size, cancelling out the scattering differences. In contrast, when the pH was raised to 9.5, a distinct peak was observed at higher *Q*, which can be attributed to well-separated scattering centers with a spacing of 12.6 nm. It is assumed that these

clusters are formed by assembly of peptides after formation of β-sheet structures. In the case of peptide monomer VK20, an intramolecular folding into β-hairpin structures and subsequent assembly into a fibrillar network was observed (Figure S6 and S7). Instead, the folded peptides within the peptide cryogels would lump together into domains. The decrease of spacing from pH 6.5 to 9.5 supports the structural changes of the clusters. It is speculated that the clusters containing assembled peptides would have larger sizes and thus the spacing between them would decrease after formation of assembled β-sheet at pH 9.5.

Furthermore, the capability of the structural function of the micropores to maintain the pH-dependent volumetric degree of swelling (Q_v) of peptide containing cryogels was investigated. The decrease of Q_v for the series of cryogels ranged between 13 ± 2% and 35 ± 10% when the pH was raised from pH 6 to 10 (Figure S8a). This indicated a buffering effect during swelling and de-swelling of the cryogels by the porous structure and by this a dimensional stability. The porous structure was confirmed in the dry state by SEM and in the swollen state by light microscopy (Figure S9). The mechanical strength of porous cryogels in the swollen state could be characterized by dynamic viscoelastic studies. A significant increase of the storage modulus G' was determined for the peptide cryogels when the pH increased from pH 6.5 to 9.5 (Figure S8b). This increase in G' can be attributed to additional physical crosslinks in the cryogels, caused by the β-sheet formation induced assembly of peptide segments.

The capability for directed shape-shifts was quantified from bending tests by the shape-fixity ratio (R_f) and the shape-recovery ratio (R_r) (see experimental part). Figure 3a shows the change of β-sheet contents of the peptide containing cryogels obtained from IR results over a pH range from 2 to 12. The amount of β-sheet increased at around pH 6 and reached a plateau at around pH 10. Accordingly, the shape-memory experiments were performed in this pH range. As shown in Figure 3b, R_f raised with increasing pH values from 8.5 to 10, which correlates with the higher content of pH-reversible netpoints (β-sheets) fixing the temporary shape. Furthermore, R_f ranges from 38 ± 5% to 90 ± 3% with higher peptide concentration because of the increased total amounts of temporary crosslinks. In addition, a cryogel solely having PEG units was unable to fix the temporary shape when the same conditions were applied as for the peptide containing cryogels. The kinetics of the shape-recovery process were explored at pH 6.5 after the temporary shape was obtained at pH 9.5. The time period for recovery was rather short and occurred within 60 min of VK1(200), VK2(100), while the recovery process for VK3(67) and VK4(50) required 180 min with recovery ratios of 75 ± 9% and 88 ± 8% respectively (Figure 3c). However, the R_r after equilibrium were independent of the peptide concentration and ranged between 90 ± 3% and 98 ± 2%. These results indicate the dependency of the recovery rate on the peptide segments and the diffusion rate of proton ions into the hydrogel interpenetrating network (IPN). In the case of VK3(67) and VK4(50), the higher amount of the aggregated peptide segments induced a lower disassembly rate, resulting in slow shape-recovery.

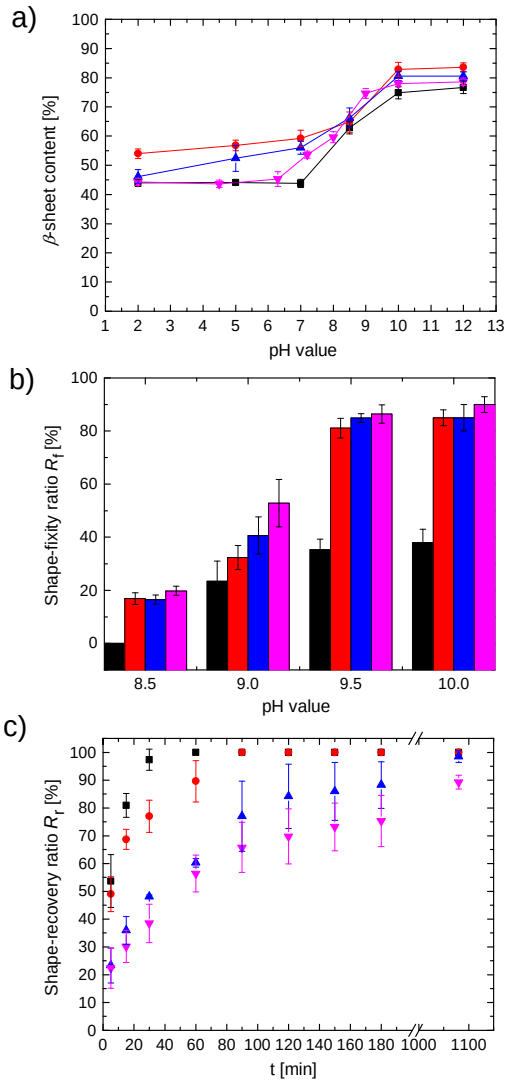

Figure 3 Quantitative characterization of conformation and shape-memory properties of peptide containing cryogels a) β-sheet content of peptide containing cryogels at varied pH conditions; b) R_f of peptide containing cryogels in the range of fixing pH from 8.5 to 10; c) Kinetics of shape-recovery of peptide containing cryogels at pH 6.5 (average values from 2nd-4th cycle). VK1(200): black square, VK2(100): red circle, VK3(67): blue up triangle, VK4(50): magenta down triangle.

All results obtained, indicate a reversible conformational transition of peptide segments acting as reversible switches and their sequential translation to trigger a pH-induced shape-shift. However, the influence of pH-induced protonation/deprotonation of peptide chains cannot be fully excluded. Therefore, a control experiment with peptide sequence NK8, which was pH-sensitive but unable to change the conformation,

was performed. The results obtained from (circular dichroism) CD and (infrared) IR measurements (Figure S10) support that NK8 adopts random coil conformation over a wide pH range. In addition, the NK2(100) cryogel did not show a SME. The conformation of NK2(100) was pH-independent, suggesting that the protonation/deprotonation of peptide segments does not contribute to the SME. The results further confirm the pH-induced conformational transition triggered folding of peptides forming β-sheet domains to act as temporary crosslinks for achieving SME in peptide containing cryogels.

CONCLUSION

A concept of sequentially coupling the functions in an IPN based hydrogel has been introduced, in which the reversible conformational change of peptide molecules incorporated in microporous architectured hydrogels is translated over several hierarchical levels via sequentially coupling functions into a reprogrammable, directed shape-shift to induce a macroscopic shape-shift. The permanent shape was defined by the covalently crosslinked component of the IPN, which also enabled dimensional stability of the macroscopic shape when deformed and upon recovery. A mechanism for the sequential coupling of the pH-sensitive cryogels could be elaborated as a control - a peptide cryogel with pH-sensitivity but without conformational change - was not capable of a shape-shift. According to this mechanism, the peptide side chains adopted predominantly β-sheet conformation and formed domains with a defined spacing

whereby they acted as additional temporary crosslinks fixing the temporary shape. Multifunctional peptides could be able to implement additional functionalities e.g. bio-functionality by using peptides, which are antimicrobial, depending on their conformation. In this way, this material system might pave the way to create smart devices for biomedical applications like an occluder for cancer treatment, which plug nourishing blood vessels of a tumor or an adaptive plaster capable of adapting to complex shapes and providing an aseptic surface.[29]

SUPPORTING INFORMATION

Supporting information is available online or from the author.

Figure S1 Synthesis scheme of peptide cryogels, Table S1 Gel content, degree of swelling and pore morphology of peptide cryogels, Figure S2 Kinetic study of conformation transition of peptide cryogels, Figure S3 WAXS characterization of peptide cryogels, Figure S4 UV spectroscopic characterization of cryogels with congo red, Figure S5 Light microscopy image of Cryogel VK4(50) after addition of Congo red solution, Table S2 Assignments of carbon of peptide cryogel VK4(50) and estimations for the contents of secondary structure, Figure S6 SANS characterization of peptide monomer VK20 solutions, Figure S7 Guinier analysis of SANS spectra of peptide monomer VK20, Figure S8 Swelling and rheological properties of peptide cryogels, Figure S9 Pore morphology of peptide cryogels, Figure S10 CD, IR spectroscopic characterization of NK8 peptide solution and peptide cryogel.

AUTHOR INFORMATION

Corresponding Author

* Prof. Dr. A. Lendlein, Corresponding author, andreas.lendlein@hzg.de

Funding Sources

This work has been financially supported by the Helmholtz Association through program-oriented funding, by the Tianjin University-Helmholtz-Zentrum Geesthacht, Joint Laboratory for Biomaterials and Regenerative Medicine, which is financed by the German Federal Ministry of Education and Research (BMBF, Grant No. 0315496) and the Chinese Ministry of Science and Technology (MOST, 2008DFA51170), as well as by the German Research Foundation (INST 121384/58-1). Zewang You is grateful for financial support by the China Scholarship Council (CSC) (Grant No. 201306140012).

ACKNOWLEDGEMENT

We acknowledge the KIT light source for provision of instruments at the beamline UV-CD12 of the Institute of Biological Interfaces (IBG2), we would like to thank the Institute for Beam Physics and Technology (IBPT) for the operation of the storage ring, the Karlsruhe Research Accelerator (KARA), and we are grateful to Bianca Posselt for the assistance in preparing the peptide cryogel samples for SRCD. We would like to thank Dr. Sebastian Busch and Prof. Martin Müller for the help of the SANS characterization at FRM II (Forschungsneutronenquelle Heinz Maier-Leibnitz, Garching, Germany) and Markus Schmitt at KIT, IBG-2, for his support in the NMR measurements.

Author contributions

AL, MB and ZY designed the study, ZY, SG, JB and QZ aquisited, ZY, SG, JB, and MB analyzed, ZY, SG, JB, MB, AU, and AL interpreted the data, ZY drafted the work and MB and AL substantially revised the manuscript. All authors approved the submitted version of the manuscript.

REFERENCES

1. Lendlein, A.; Trask, R. S., Multifunctional materials: concepts, function-structure relationships, knowledge-based design, translational materials research. *Multifunct. Mater.* **2018,** 1, (1), 010201.

2. Yu, Y. L.; Nakano, M.; Ikeda, T., Directed bending of a polymer film by light - Miniaturizing a simple photomechanical system could expand its range of applications. *Nature* **2003,** 425, (6954), 145-145.

3. White, T. J.; Broer, D. J., Programmable and adaptive mechanics with liquid crystal polymer networks and elastomers. *Nat. Mater.* **2015,** 14, 1087.

4. Tamesue, S.; Takashima, Y.; Yamaguchi, H.; Shinkai, S.; Harada, A., Photoswitchable Supramolecular Hydrogels Formed by Cyclodextrins and Azobenzene Polymers. *Angew. Chem., Int. Ed.* **2010,** 49, (41), 7461-7464.

5. Weigelt, S.; Busse, C.; Petersen, L.; Rauls, E.; Hammer, B.; Gothelf, K. V.; Besenbacher, F.; Linderoth, T. R., Chiral switching by spontaneous conformational change in adsorbed organic molecules. *Nat. Mater.* **2006,** 5, (2), 112-117.

6. Johnson, R. R.; Johnson, A. T. C.; Klein, M. L., Probing the structure of DNA-carbon nanotube hybrids with molecular dynamics. *Nano Lett.* **2008,** 8, (1), 69-75.

7. Löwenberg, C.; Balk, M.; Wischke, C.; Behl, M.; Lendlein, A., Shape-memory hydrogels: evolution of structural principles to enable shape switching of hydrophilic polymer networks. *Acc. Chem. Res.* **2017,** 50, (4), 723-732.

8. Osada, Y.; Matsuda, A., Shape memory in hydrogels. *Nature* **1995,** 376, (6537), 219-219.

9. Inomata, K.; Terahama, T.; Sekoguchi, R.; Ito, T.; Sugimoto, H.; Nakanishi, E., Shape memory properties of polypeptide hydrogels having hydrophobic alkyl side chains. *Polymer* **2012,** 53, (15), 3281-3286.

10. Balk, M.; Behl, M.; Noechel, U.; Lendlein, A., Shape-Memory Hydrogels with Switching Segments Based on Oligo(omega-pentadecalactone). *Macromol. Mater. Eng.* **2012,** 297, (12), 1184-1192.

11. Miyata, T.; Uragami, T.; Nakamae, K., Biomolecule-sensitive hydrogels. *Adv. Drug Deliv. Rev.* **2002,** 54, (1), 79-98.

12. Ehrick, J. D.; Deo, S. K.; Browning, T. W.; Bachas, L. G.; Madou, M. J.; Daunert, S., Genetically engineered protein in hydrogels tailors stimuli-responsive characteristics. *Nat. Mater.* **2005,** 4, (4), 298-302.

13. Yuan, W.; Yang, J.; Kopečková, P.; Kopeček, J., Smart Hydrogels Containing Adenylate Kinase: Translating Substrate Recognition into Macroscopic Motion. *J. Am. Chem. Soc.* **2008,** 130, (47), 15760-15761.

14. Guo, W.; Lu, C.-H.; Orbach, R.; Wang, F.; Qi, X.-J.; Cecconello, A.; Seliktar, D.; Willner, I., pH-Stimulated DNA Hydrogels Exhibiting Shape-Memory Properties. *Adv. Mater.* **2015,** 27, (1), 73-78.

15. Skrzeszewska, P. J.; Jong, L. N.; de Wolf, F. A.; Stuart, M. A. C.; van der Gucht, J., Shape-Memory Effects in Biopolymer Networks with Collagen-Like Transient Nodes. *Biomacromolecules* **2011,** 12, (6), 2285-2292.

16. Ulijn, R. V.; Smith, A. M., Designing peptide based nanomaterials. *Chem. Soc. Rev.* **2008,** 37, (4), 664-675.

17. Lowik, D. W. P. M.; Leunissen, E. H. P.; van den Heuvel, M.; Hansen, M. B.; van Hest, J. C. M., Stimulus responsive peptide based materials. *Chem. Soc. Rev.* **2010,** 39, (9), 3394-3412.

18. I. Lozinsky, V., Cryogels on the basis of natural and synthetic polymers: preparation, properties and application. *Russ. Chem. Rev.* **2002,** 71, (6), 489-511.

19. Petrov, P.; Petrova, E.; Tsvetanov, C. B., UV-assisted synthesis of super-macroporous polymer hydrogels. *Polymer* **2009,** 50, (5), 1118-1123.

20. Barrow, M.; Zhang, H., Aligned porous stimuli-responsive hydrogels via directional freezing and frozen UV initiated polymerization. *Soft Matter* **2013,** 9, (9), 2723-2729.

21. Zhang, P.; Behl, M.; Peng, X.; Razzaq, M. Y.; Lendlein, A., Ultrasonic Cavitation Induced Shape-Memory Effect in Porous Polymer Networks. *Macromol. Rapid Commun.* **2016,** 37, (23), 1897-1903.

22. Schneider, J. P.; Pochan, D. J.; Ozbas, B.; Rajagopal, K.; Pakstis, L.; Kretsinger, J., Responsive Hydrogels from the Intramolecular Folding and Self-Assembly of a Designed Peptide. *J. Am. Chem. Soc.* **2002,** 124, (50), 15030-15037.

23. Keiderling, U., The new 'BerSANS-PC' software for reduction and treatment of small angle neutron scattering data. *Appl. Phys. A: Mater. Sci. Process.* **2002,** 74, (1), s1455-s1457.

24. Kikhney, A. G.; Svergun, D. I., A practical guide to small angle X-ray scattering (SAXS) of flexible and intrinsically disordered proteins. *FEBS Letters* **2015,** 589, (19PartA), 2570-2577.

25. Barth, A., Infrared spectroscopy of proteins. *Biochim. Biophys. Acta, Bioenerg.* **2007,** 1767, (9), 1073-1101.

26. Kubelka, J.; Keiderling, T. A., The Anomalous Infrared Amide I Intensity Distribution in 13C Isotopically Labeled Peptide β-Sheets Comes from Extended, Multiple-Stranded Structures. An ab Initio Study. *J. Am. Chem. Soc.* **2001,** 123, (25), 6142-6150.

27. You, Z.; Behl, M.; Löwenberg, C.; Lendlein, A., pH-sensitivity and Conformation Change of the N-terminal Methacrylated Peptide VK20. *MRS Adv.* **2017,** 2, (47), 2571-2579.

28. Leonard, Sarah R.; Cormier, Ashley R.; Pang, X.; Zimmerman, Maxwell I.; Zhou, H.-X.; Paravastu, Anant K., Solid-State NMR Evidence for β-Hairpin Structure within MAX8 Designer Peptide Nanofibers. *Biophys. J.* **2013,** 105, (1), 222-230.

29. Babii, O.; Afonin, S.; Ishchenko, A. Y.; Schober, T.; Negelia, A. O.; Tolstanova, G. M.; Garmanchuk, L. V.; Ostapchenko, L. I.; Komarov, I. V.; Ulrich, A. S., Structure–Activity Relationships of Photoswitchable Diarylethene-Based β-Hairpin Peptides as Membranolytic Antimicrobial and Anticancer Agents. *J. Med. Chem.* **2018,** 61, (23), 10793-10813.

TOC graphic